

Compact Dielectric Elastomer Linear Actuators

Huichan Zhao, Aftab M. Hussain, Mihai Duduta, Daniel M. Vogt, Robert J. Wood,*
and David R. Clarke*

The design and fabrication of a rolled dielectric elastomer actuator is described and the parametric dependence of the displacement and blocked force on the actuator geometry, elastomer layer thickness, voltage, and number of turns is analyzed. Combinations of different elastomers and carbon nanotube electrodes are investigated and optimized to meet performance characteristics appropriate to tactile display applications, namely operation up to 200 Hz with a combination of a 1 N blocked force and free displacement of 1 mm, all within a volume of less than 1 cm³. Lives in excess of 50 000 cycles have been obtained. Key to meeting these objectives is control of the multilayering fabrication process, the carbon nanotube electrode concentration, the selection of a soft elastomer with low viscous losses, and a proof-testing procedure for enhancing life cycle reliability.

1. Introduction

The landmark papers by Pelrine et al. marked the beginning of the use of dielectric elastomer (DE) actuators (and sensors) for soft robotics.^[1] They showed that a voltage applied through the thickness of a soft material could produce large strains as a result of the Maxwell stress between charges on the two electrodes. Their work and subsequent reports^[2] have shown that DE-based actuators are particularly attractive for many soft robotic applications because they exhibit large energy densities with large strains and muscle-like response times.^[1b,3] In addition, being mechanically soft they are intrinsically compatible with human skin, a factor that becomes important for dynamic tactile applications.^[4]

The most commonly investigated geometry used to demonstrate the underlying physics of DE actuation, as well as several device concepts, has been a prestretched elastomer sheet with electrodes coated on both sides.^[5] The electromechanics of this “thin-film” geometry has been well developed, a variety of fabrication techniques implemented, and the basis for material


selection has been demonstrated.^[6] However, the actuation forces that these thin-film actuators can produce are relatively small, typically in the range of mN for an electric field of $\approx 10 \text{ MV m}^{-1}$, even for elastomer compositions that do not require prestretching, such as the acrylics^[7] and the bottle-brush elastomers.^[8] They are also of limited value as an engineering actuator since the electrostatic stress creates a biaxial strain in response to a through-thickness applied voltage, whereas many traditional and practical actuators are based on uniaxial displacements or bending strains. These limitations have been overcome with the evolution of a number of designs for con-

verting the electric field-induced biaxial strain to linear motion and amplifying the force output. Stacking multiple layers of DE films is one common technique to generate axial contraction and bending unimorphs or bimorphs.^[7a,9] Folding a long sheet of DE (often with multiple folds) is another method for generating large contractile forces.^[9b] A hydraulically coupled actuator, also based on the creation of an electric field-induced Maxwell stress has recently been demonstrated.^[10] In this novel device, the attraction between electrostatic charges on a polymer sheet is transformed to a fluid displacement but without the requirement of a stretchable polymer or electrodes. As with the dielectric elastomers, the device contracts in the direction of the applied field. An alternative geometry, a rolled DE sheet not only converts the biaxial expansion into the linear motion along the axis of the roll, but also amplifies the force output by simply increasing the number of turns, as will be shown below. However, the majority of previously demonstrated devices have required prestraining of the elastomer together with a rigid structure to maintain the prestrain to achieve large strains before dielectric breakdown.

The advantages of the rolled configuration as a linear actuator have been recognized previously. For instance, the “spring-roll” structures proposed by Pei et al. utilize a precompressed spring as a way to prestrain the elastomer layers and have been applied in several robotic applications.^[11] Like other prestrained DE actuators made of commercial VHB elastomers (an acrylic adhesive tape from 3M Co.), spring-roll actuators exhibit large strains and forces but suffer from limited bandwidth (usually <10 Hz). Others have fabricated roll actuators that do not use prestraining in order to simplify the fabrication process. In these examples, the novelty has largely been in the choice of electrodes. For example, silicone rubber with corrugated metallic electrodes has been used to produce linear actuators in large quantities based on industrial roll-to-roll fabrication.^[12]

Dr. H. Zhao, Dr. A. M. Hussain, M. Duduta, D. M. Vogt, Prof. R. J. Wood, Prof. D. R. Clarke
School of Engineering and Applied Sciences
Harvard University
Cambridge, MA 02138, USA
E-mail: rjwood@seas.harvard.edu; clarke@seas.harvard.edu

Dr. H. Zhao, M. Duduta, D. M. Vogt, Prof. R. J. Wood
Wyss Institute for Biologically Inspired Engineering
Harvard University
Cambridge, MA 02138, USA

 The ORCID identification number(s) for the author(s) of this article can be found under <https://doi.org/10.1002/adfm.201804328>.

DOI: 10.1002/adfm.201804328

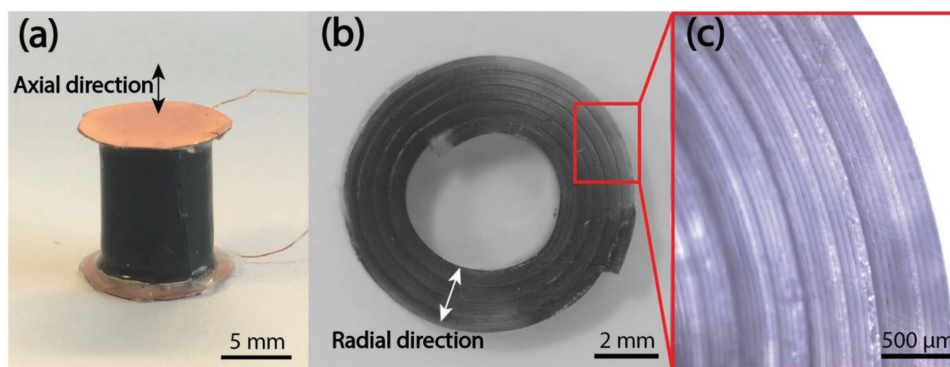


Figure 1. a) A fully assembled DE linear roll actuator bonded to metal end-supports to facilitate force and displacement measurement. b) End view of a five-turn rolled actuator, each turn consisting of ten elastomer layers. c) Higher magnification image of the cross section indicating individual elastomer and electrode layers. The latter appear as thin dark rings.

The actuators reported were typically several centimeters high but were capable of less than 3% strain, presumably being limited by the stiffness of both the metal electrodes and the elastomer used. A different approach to generate large actuation strain has been using thin-walled cylinders of the VHB film with periodic stiff rings along the length to convert the biaxial strain in the film to a uniaxial strains.^[13] Nevertheless, roll-based DE linear actuators, despite many potential applications and options for construction, still suffer from complicated fabrication techniques (e.g., prestraining a roll structure, electrode application onto large areas, potential slip between layers of the rolled structure, etc.), poor performance (i.e., either small strain or low bandwidth, or high driving voltage, etc.), and a lack of a model for the performance dependence on the geometric parameters and material properties.

In this work, we report an improved method for fabricating a roll actuator for tactile applications with an emphasis on both geometric and material parameters to gain an understanding of actuator design, including end effects and frequency dependencies. Specifically, we targeted a lightweight (<1 g), low-profile (total height less than 1 cm) actuator (Figure 1 and Video S1, Supporting Information) with a combination of high force ($\approx 1 \text{ N cm}^{-2}$), large strain (10%), and high bandwidth (DC to 200 Hz) operating at voltage of 1000 V or less. This combination of traits has not been demonstrated in existing actuator technologies, for example, electromagnetic motors, piezoelectric actuators, or pneumatic devices. It also has not been realized by other DE actuators operating at 1000 V or below. The frequency range corresponds to the range shown to be perceptible in touch experiments.^[14] As will be described, our actuator is based on a combination of improvements in modeling and design, elastomer selection, compliant electrodes based on percolative networks of carbon nanotubes (CNTs), and processing innovations in producing elastomer/electrode multilayers.

In the following section, we will first describe the underlying actuator concept, an analytical model for the actuator performance that relates geometric parameters, and material properties to actuator displacement and blocked forces. In Section 3, we will describe our fabrication procedures and material selection, and report on the performance of the linear actuators in both static and dynamic modes. Finally, we discuss the results and give a brief conclusion.

2. Concepts and Modeling

2.1. Principle of Operation

The concept underlying the actuator design is to convert the biaxial stretching of a thin sheet induced by an applied voltage into a uniaxial force by wrapping the elastomer into a roll. Ideally, the friction and adhesion between the individual layers and turns prevents the unwinding of the layers, constraining the displacements to act primarily in the axial direction and minimize them in the radial direction. Furthermore, by creating a multilayered rolled structure, the axial forces produced increase with the number of layers. The actuator consists of a circularly multilayered structure with N layers of electrode/elastomer composite, where the thickness of each elastomer layer is d and the electrode thickness is negligible (Figure S1, Supporting Information). The electrodes are connected interdigitally so every alternate electrode is connected to high voltage and the other set to ground. As the electric field is applied through the thickness of the rolls, it induces a Maxwell stress ($P = \epsilon E^2$) in the radial direction causing the structure to contract in the radial direction and extend in the axial direction to maintain a constant volume of the elastomer (elastomers are incompressible). If the structure is fixed at one end and blocked at the other along the axial direction, it will generate an axial (blocked) force, otherwise if the end is free the actuator will extend in the axial direction.

2.2. Static Modeling

An analytical electromechanical model for the static deformation of the axial actuator is presented to establish the parametric dependence of the axial displacement and blocked force with applied voltage. The purpose is twofold: first to establish the parametric dependencies and, second, to compare with a COMSOL model that can take into account a variety of practical constraints encountered in fabricating and evaluating actuators, such as end cap effects. Previous models of rolled DE actuators either consider only a single layer or were numerical analyses only.^[15]

In the analytical model, a number of simplifying assumptions are made to derive a tractable model. These can be relaxed

in the COMSOL model, which requires less simplification. The simplifying assumptions are that the rolled structure is replaced by a series of concentric cylindrical shells, the elastomers are homogeneous, incompressible and linear elastic, and both the radius of each layer and the actuator height are significantly larger than the thickness of the individual elastomer layers. In all cases we assume that the electrode thickness is negligible, as we have found to be the case for our material/electrode combinations. It is also assumed that there is no delamination between individual layers, so that elastic and electric continuity exists across each layer. In the analytical model, two other assumptions are made. The cross section is assumed not to depend on the axial position and so there are effectively no ends. The other is that the electric field change caused by deformation is ignored in the model as only small strains are considered.

Starting with the equations for the force equilibrium of an arbitrary element of layer N , and by applying appropriate boundary conditions, we analytically solved the displacement field of the whole structure when an electric field is applied (Section 1 in the Supporting Information describes the detailed derivation). To solve the various integration constants and investigate how the displacement and blocked force change with varying both geometric parameters and materials properties, the equations were solved using Matlab. The two limits to the actuator response, corresponding to free displacement, ΔL and blocked force, $|\sum_1^N F_n|$ can be determined from the interaction stiffness, k , which expresses the interaction between the rolled structure and an external load and interaction between adjacent layers. The free displacement is when $k = 0$ and $k = 20\,000\text{ N m}^{-1}$ (an arbitrarily large number) corresponds to the blocked limit. By varying the model parameters, we obtain the following simple approximations:

$$\Delta L \approx \frac{1}{2} \frac{\epsilon_p \left(\frac{V}{d}\right)^2}{Y} L \quad (1)$$

$$|\sum_1^N F_n| \approx \frac{1}{2} \epsilon_p \left(\frac{V}{d}\right)^2 S \quad (2)$$

where L is the height of the rolled structure, V is the voltage being applied, ϵ_p is the permittivity of the elastomer, Y is Young's modulus of the elastomer, and S is the total cross-sectional area of the roll structure.

These equations indicate that when V is held constant decreasing the layer thickness increases both the free unconstrained axial displacement and the blocked force. Similarly, increasing the actuator length increases the attainable free displacement and increasing the number of layers increases the blocked force. Also, it is worth noting that, the axial displacement and the axial blocked force are half those of a stacked actuator of the same dimensions, due to the fact that the circumferential strains are not constrained. In the roll configuration, provided the roll diameter is much larger than the thickness of the individual multilayers, the force scales with the cross-sectional area and only weakly depends on the roll diameter.

The analytical results were compared with those of a coupled electromechanical COMSOL module simulation. The simulation takes into account shear forces between layers and a no-slip condition at both ends to represent the actuator being attached to end caps that prevent radial motion at the ends. They also include the possibility that the elastomers are not electroded all the way to the ends. To illustrate the comparison, the free displacement and blocked force of a 54 layer multicylinder actuator with an active length of 10 mm, inactive length of 2 mm, a layer thickness of 50 micrometers, and Young's modulus of 80 kPa, corresponding to one of the actuators fabricated, was simulated. The results are shown in **Figure 2**. The analytical predictions of the displacements and forces are very consistent with the simulation results, and both show that the free displacement and blocked force are proportional to the square of applied voltage. There are slight differences in that the analytical model predicts that the displacements are somewhat higher than the simulations and the blocked force of the analytical model is a little lower (Figure 2a,c) at the highest fields. Figure 2b shows the simulated displacement of the entire structure in the z (axial) and r (radial) directions for the free motion. Figure 2d shows the simulated z direction and r direction displacements for the blocked simulation. For the free displacement condition, the outer surface contracts and inner surface bows out, whereas in the blocked force condition, the outer surface bulges out with a smaller inner surface bowing. In essence, the end caps have, as expected, the effect of constraining the radial displacements near the ends. They also have the effect of bending the outer wall in the free axial displacement condition, resulting in lower displacement, while in the blocked condition they limit the outer bulging increasing the blocked force.

3. Results

3.1. Fabrication Process

The fabrication process consists of two basic processes: i) multilayering (**Figure 3a**) and ii) rolling (**Figure 3b,c**). In the multilayering process, individual thin sheets of elastomer were prepared by spin casting onto an acrylic substrate, a nonadhesive material used for support. Elastomer films in the range of 20–50 μm of uniform thickness could be reliably produced at spin rates between 1000 and 2000 rpm. The elastomer was then cured by heating to 70 $^{\circ}\text{C}$ for 20 min. Electrodes consisting of a mat of single wall CNTs were transferred by stamping from a polytetrafluoroethylene (PTFE) filter onto the elastomer layer through a mask (laser cut from silicone release film from Drytac, Inc.) to form the desired electrode shape. Multilayers were then formed by stacking, ensuring that the electrode tabs were aligned in alternating layers to produce an interdigitated structure, with the number of layers needed for the designed actuator behavior. The multilayer structure was then given a final cure at 70 $^{\circ}\text{C}$.

To form the actuator, long strips were cut from the multilayered elastomer–electrodes sheet leaving the CNT electrode tabs exposed to both sides of the long strip. The strips were then rolled and each electrode side forms a flat surface. Strips could also be oriented in a head-to-end form and rolled into a cylinder with more turns. Silver paste (Electron Microscopy Sciences,

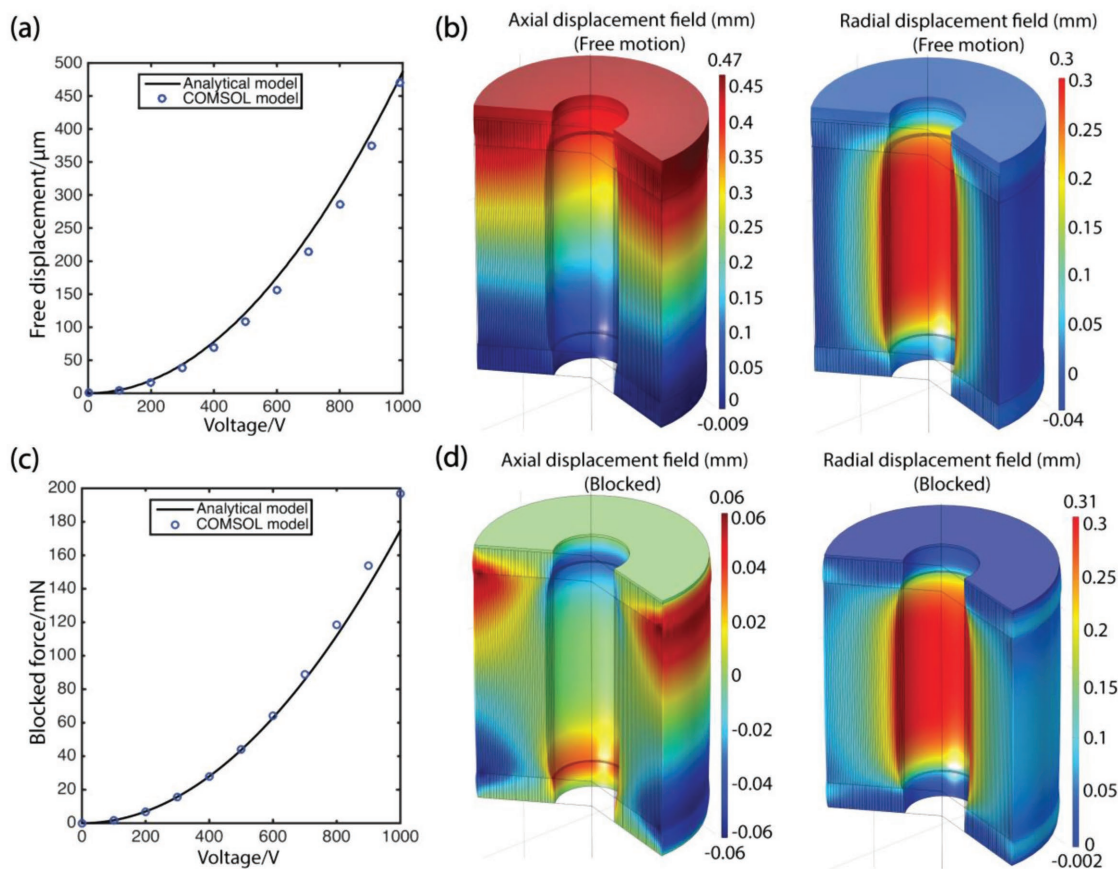


Figure 2. a,c) Comparison between the analytical and simulation models of the voltage dependence of the free displacement and blocked force. b) Axial and radial displacement fields, respectively, under zero load. d) Axial and radial displacement fields under the blocked end condition. The actuator had an active length of 10 mm. The displacement fields shown were simulated at 1000 V.

Inc.) was applied to the flat surfaces with CNTs exposed, so as to create electrical connections to the interdigitated sets of electrodes. Finally, a rigid plastic with copper tape or carbon on one side was glued to the ends of the actuator to provide a base and a contacting surface.

3.2. Material Selection and Geometric Parameters

Although the fabrication process could be applied to create actuators using a variety of elastomers, silicone elastomers were selected because of a combination of ease of processing and physical properties, primarily with the ability to spin cast them into thin sheets, their elastic properties, and their low viscoelastic losses. Specifically, a low elastic modulus is required to achieve high strains and low viscoelastic losses are required to operate at higher frequencies. For these reasons, silicone elastomers consisting of mixtures of Sylgard 184 (Dow Corning) and Ecoflex 0030 (Smooth-On) were investigated. These two commercial elastomers were selected based on their reported properties. Then, based on the combination of elastic modulus and low viscoelasticity ($\tan \delta$), an equal volume mixture of the two was selected (see Experimental Section for details of materials properties).

To investigate how geometric parameters affect the performance of the rolled linear actuator, a series of actuators with different dimensions were fabricated. The elastomer layer thickness was varied by varying the spin-coating speeds ranging from 1000 to 2000 rpm. To alter the actuator height, the size of the masks (see Figure S2, Supporting Information) used for stamping electrodes was varied. The number of turns in the actuator was varied by changing the number of rectangular strips rolled together. **Table 1** summarizes the parameter combinations investigated. Together, we investigated four variables: varying height, varying turns, varying thickness, and varying material properties that might affect dynamic performance.

3.3. Soft Breakdown Characteristics

Before characterizing the static and dynamic behavior of the actuators, they were first proof tested to “burn” out low-resistance breakdown paths. In this process, the voltage was stepped up to 1000 in 100 V steps, each lasting one second. Both the current drawn and the free displacement were measured concurrently. The leakage current (which is defined as the current going through the actuator when the voltage is held constant) can exhibit short erratic pulses in the first run and then

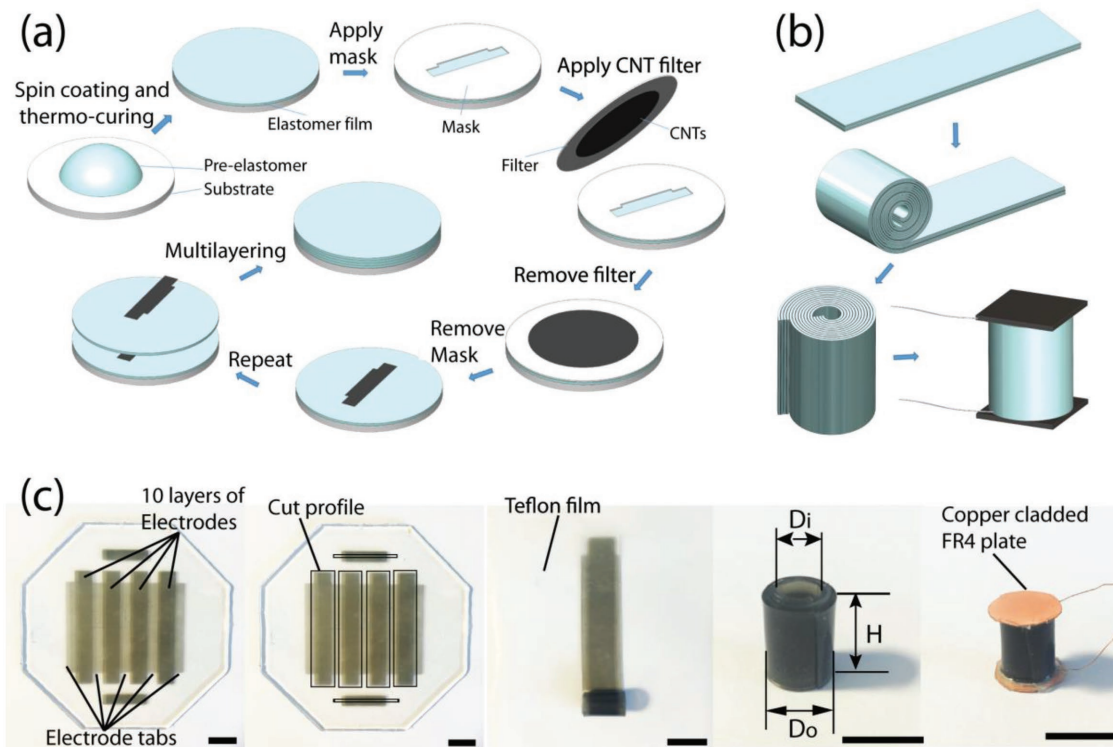


Figure 3. Fabrication method. a) Sequence of operations to produce a multilayer of elastomer and CNT electrodes. b) The rolling process (the fully assembled actuator with flat caps glued to the ends is shown in the right figure.). c) Photographs at different stages in the fabrication. The dark horizontal rectangles in the first picture of panel (c) are used for thickness measurement by confocal microscopy. (scale bars indicate 1 cm.)

gradually decreases to negligible values with further cycling. This phenomenon is a form of “soft breakdown.” Breakdown in polymer dielectrics is associated with the burning out of a conducting channel within the dielectric and a local region of the electrodes. (More recently, it has been described as a “self-clearing” process.)^[16] **Figure 4** shows the proof testing of actuator 2 (Table 1) for the first, second, third, fourth, and tenth run, respectively. After the tenth run, we repeatedly activated the actuator from 0 to 1000 V for 50 000 times at various frequencies (200, 60, 10, and 1 Hz), there was no evidence for further “soft-breakdown,” and both the current and the displacement subsequently remained unchanged as the tenth run. The final failure was by irreversible electrical breakdown.

3.4. Static Response

The static performance of the actuators was determined using a similar voltage ramping procedure as used in the proof testing, except each voltage step was held for 20 s to record any time dependence of the measured displacements and forces. A total of 100 data points at a sampling rate of 5k Hz were recorded at each step so that their averages could be determined. As illustrated in **Figure 5**, both the free displacement and blocked force of the linear actuators follow the expected parabolic dependence of applied voltages, as predicted by the static model in Section 2. The data in **Figure 5a,b** confirmed that decreasing the layer thickness (from 50 to 35 to 25 μm) enabled both a

higher free displacement as well as a larger blocked force. However, as we further decreased layer thickness below 25 micrometers, we were not able to self-clear the actuators—the presence of defects results in a permanent leakage current even after more than 50 cycles through the self-clearing process. Another geometric parameter is the active length of the actuator, the length of the actuator electroded. Consistent with the simple model, larger free displacements could be achieved with increasing the active height of the actuator (**Figure 5c**). Similarly, with increasing number of turns, the blocked force increased, while the free displacement is unaffected (**Figure 5d**). Converting the number of turns into an area, the blocked force was found to increase linearly with the cross-sectional area of the actuator.

Together, the dependence of the static forces and displacements on the geometric factors, such as actuator length, number of turns, and layer thicknesses, provides the basic rules for choosing the actuator parameters to meet different requirements in designing compact actuator devices.

3.5. Dynamic Response

Measurements of the displacement at frequencies from 1 to 500 Hz were made for five different combinations of elastomer and electrode conductivity (Table 1, actuators 12–16, **Figure 6a**). Among the five actuators, three of them (actuators 12, 13, and 15) exhibited a broad, almost frequency-independent response up to ≈ 100 Hz, followed by amplitude increases, and then above

Table 1. Actuator parameters and materials.

	Actuator #	Height ^{a)} [mm]	Turn #	Spin speed [rpm]	Elastomer	Electrode ^{b)}	R ^{c)} [MΩ]	C ^{d)} [nF]	RC [ms]	Layer #	Weight ^{e)} [g]
Height	1	6	5	1500	Mixture (1:1)	2 × CNT	0.83	1.4	1.1	10	0.40
	2	8	5	1500	Mixture (1:1)	2 × CNT	0.60	2.0	1.2	10	0.50
	3	10	5	1500	Mixture (1:1)	2 × CNT	0.42	2.4	1.0	10	0.60
	4	12	5	1500	Mixture (1:1)	2 × CNT	0.50	2.6	1.3	10	0.70
Turns	5	8	3	1500	Mixture (1:1)	2 × CNT	1.43	0.7	1.0	10	0.24
	6(2)	8	5	1500	Mixture (1:1)	2 × CNT	0.60	2.0	1.2	10	0.50
	7	8	7	1500	Mixture (1:1)	2 × CNT	0.36	2.9	1.0	10	0.72
	8	8	9	1500	Mixture (1:1)	2 × CNT	0.50	4.6	2.3	10	1.05
Thickness	9	8	5	1000	Mixture (1:1)	2 × CNT	0.50	1.9	1.0	10	0.67
	10(2)	8	5	1500	Mixture (1:1)	2 × CNT	0.60	2.0	1.2	10	0.50
	11	8	5	2000	Mixture (1:1)	2 × CNT	0.45	3.2	1.4	10	0.29
Dynamics	12	8	5	1500	Mixture (1:1)	3 × CNT	0.25	1.7	0.4	10	0.50
	13(2)	8	5	1500	Mixture (1:1)	2 × CNT	0.60	2.0	1.2	10	0.50
	14	8	5	1500	Mixture (1:1)	1 × CNT	2.00	2.5	5.0	10	0.50
	15	8	5	1500	Sylgard 40:1	2 × CNT	0.63	1.9	1.2	10	0.67
	16	8	5	1500	Sylgard 50:1	2 × CNT	1.25	1.8	2.3	10	0.75

^{a)}Active height; ^{b)}number of layers of stamped CNT used to form the electrodes; ^{c)}measured in 100 V steps up to 1000 V and recording the peak current values; ^{d)}determined from direct current measurements made as a function of voltage at low frequencies (1–10 Hz) voltage; ^{e)}the weight includes all elastomer/electrodes composite and excludes the top and bottom plate.

which the response rolled off quickly. The detailed response above 100 Hz depended on the elastomer and electrode combination, with the highest resonant frequency being exhibited by actuator 12, which has both the lowest $\tan \delta$ and RC time constant among the five. Notably, each exhibited two discernable resonant frequencies f_{r1} and f_{r2} with a relationship $f_{r1} = 2f_{r2}$, as predicted by our dynamic model described in Section 2 in the Supporting Information.

The other two actuators (actuators 14 and 16) exhibited severe damping, which resulted in low bandwidth (10 and 13 Hz, respectively). Actuator 14, with a large RC time constant of 5 ms and low $\tan \delta$ of 0.10, exhibited high damping, mainly due to electrical damping; while actuator 16 with small RC time constant (2.3 ms), and a high $\tan \delta$ (0.30) exhibited high damping mainly due to mechanical damping. The highly electrically damped actuator nevertheless exhibited one resonance. The displacement response to a voltage step was also revealing as shown in Figure 6b for a sudden voltage step of 1000 V. As with the frequency response, three actuators with both low RC time constants and low $\tan \delta$ achieve fast response times and exhibit underdamped responses with overshoots and oscillations, while the other two have overdamped responses with longer response times and no overshoots. Note that even though the actuator with highest density of CNTs exhibited the best dynamic performance in terms of low damping, it could only be self-cleared at up to 200 V, which limited its static performance.

We also measured the actuators' dynamic response in the blocked configuration. In contrast to the free displacement response, the blocked force frequency response (Figure 6c) monotonically decreases with increasing frequency, which is consistent with our predictions. In this case, the RC time

constant plays a more important role in the bandwidth: actuator 12 with a 0.4 ms RC time constant achieves the maximum bandwidth, actuators 13, 15, and 16 have intermediate bandwidths (50–150 Hz), and actuator 14 has the smallest bandwidth of the five. The step response (Figure 6d) exhibits similar results with actuator 14 having the largest rise time.

Table 2 summarizes the key properties and dynamic performance of the five actuators. When the actuator is in contact with a soft elastic object (e.g., skin), the dynamic bandwidth will be intermediate between those of the free moving configuration and the blocked configuration, depending on the stiffness of the object. For the five actuators of varying combinations, actuator 13 exhibits high bandwidth in both configurations, indicating that, when used for as a haptic actuator, it has the capability of generating high-frequency vibrations.

3.6. Dynamic Response Analysis

The measured frequency responses show a clear dependence on the elastomer used and the resistance of the electrodes. As suggested by the values of the RC time constants calculated, the actuator frequency response depends on both its electrical characteristics and the elastomer viscoelasticity. The frequency response data suggests that a relatively simple spring-dashpot-mass system can account for the effects of elasticity, damping, and inertia of the elastomer/electrode structure. This is shown schematically in **Figure 7a** where the input is the applied voltage and output is the displacement or the contact force, depending on the boundary conditions assumed.

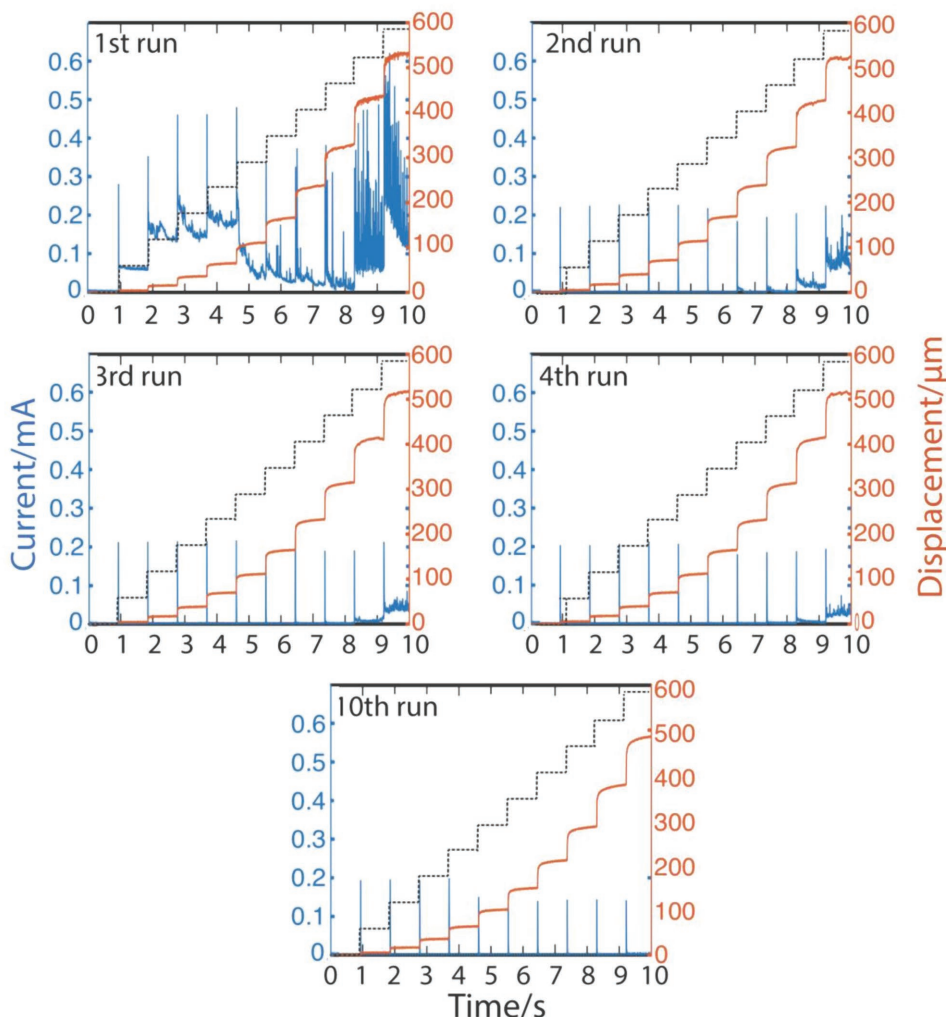


Figure 4. Displacement and drawn current as the voltage level was increased in 100 V steps every 10 s, for the first four and the tenth cycles. The current spikes are indications of “soft” electrical breakdown. With increasing voltage and number of voltage cycles, they decrease until no more electrical breakdown occurs. The actuators were then ready for characterization.

The actuator is assumed to consist of three subsystems: a first-order linear time-invariant (LTI) system with an electrical resistance and capacitance representing the electrical circuit of the actuator; a nonlinear time invariant system representing the electric field-induced force in the axial direction; and a second-order LTI system representing the mechanical response of the actuator. For the free displacement condition, the third subsystem consists of a damper, a mass, and a spring. For the blocked force condition, there is a constraint that the end displacement is zero, thus the blocked force is equivalent to the output of the second subsystem. Detailed derivation of the model is described in Section S2, relating the dynamic response of the system to the material properties (Young’s modulus Y , viscoelastic indicator $\tan \delta$, density ρ), electrical properties (R , C) as well as geometric parameters (Height L , diameter D). The predicted resonant frequencies and damping ratio can be calculated as:

$$f_{r1_predicted} = \frac{1}{2\pi} \sqrt{\frac{2Y}{\rho L^2}}, f_{r2_predicted} = 1/2 f_{r1_predicted} \quad (3)$$

$$\xi_{predicted} = \frac{1}{\sqrt{2Y\rho L^2}} \frac{Y - 2\pi^2 \rho L^2 f^2}{2\pi f} \tan \delta \quad (4)$$

in which f means the frequency at which $\tan \delta$ was measured. Substituting the parameters of actuators 12, 13, and 14 ($Y = 77.5$ kPa, $L = 8$ mm, $\rho = 1050$ kg m⁻³, and $\tan \delta = 0.34$ at 100 Hz), we get $f_{r1_predicted} = 241$ Hz and $\xi_{predicted} = 0.34$, which is close to our experimental results ($f_{r1} = 240, 180$, and 260 Hz, respectively, for actuators 12, 13, and 14, and all three are underdamped). To further explain and explore how the electrical damping and mechanical damping interact and affect the system’s dynamic response, we used Matlab to simulate the frequency sweep of free displacement and blocked force at different RC and ξ values (Figure 7b,c). The simulated results are very consistent with our experimental results in Figure 6, meaning that our dynamic model, though simple, is an effective representation for predicting the dynamic performance of an actuator in terms of the measured material properties, geometries, and electrical parameters.

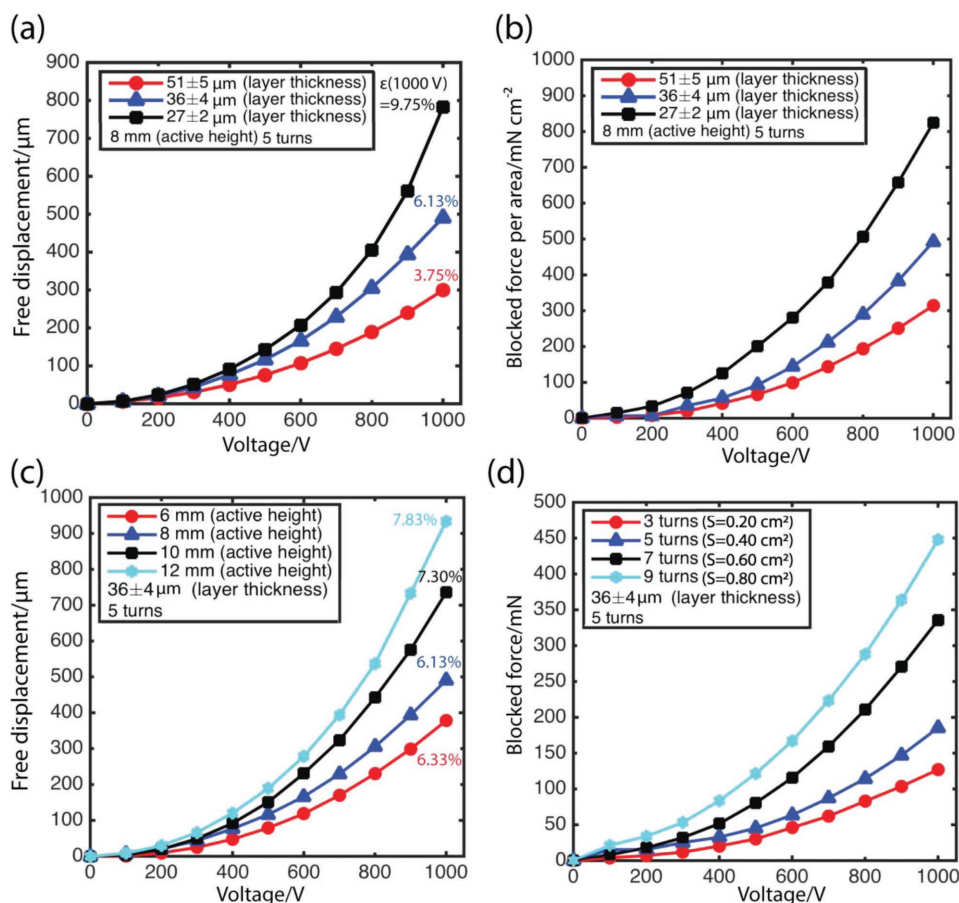


Figure 5. Measured free displacements and blocked force as a function of voltage under static conditions. a) Displacement and b) blocked force for the indicated elastomer layer thickness. c) Displacement as a function of active height. d) Blocked force as a function of number of turns of the roll. In each case, the data fit a parabolic dependence on voltage as predicted by Equation 2.

4. Discussion

Integral to the successful demonstration of these actuators has been the development of a flexible manufacturing approach based on multilayering elastomers and CNT electrodes that create strong adhesion between the electrodes and the elastomer layers.^[7a] The use of percolative CNT networks as electrodes has two advantages. The first is that they are very thin and mechanically compliant so that their stiffness does not noticeably constrain the electric field-induced expansion of the elastomer. The second is that there are physical gaps between the individual CNTs through which the elastomer layers can bond, forming strong interlayer adhesion. (Electrodes made of carbon particles tend to be much thicker in order to ensure electrical percolation and consequently can limit the lateral strain, and limit adhesion between the adjoining elastomer layers.) The use of sequential spin coating, electrode deposition, and curing though practical is not ideal, as it is time-consuming. For this reason, in this work we have adopted rather conservative maximum electric fields so we can produce actuators with high yield. We have, as part of this work, demonstrated that much thinner elastomers can be produced by spin coating but imperfections, such as small dirt particles and air bubbles entrapped during spin coating, currently limit the manufacturing yield since they are

prone to premature dielectric breakdown. We anticipate that using a roll-to-roll elastomer sheets would not only decrease the overall fabrication time but also enable thinner, more uniform dielectrics to be used with consequentially greater reliability at high fields.

As described earlier, we have also found that the “proof testing” procedure in which the voltages are increased in steps to a maximum value and repeated for a few cycles is beneficial in producing long cycle lives. The explanation for these “soft breakdowns” in terms of a “self-clearing” process originating from imperfections in the electrodes appears reasonable. Without being able to visually observe the events causing the current spikes we cannot establish the mechanism, but we believe that breakdown is stochastic and initiates from the ends of individual CNTs connected to the percolating electrode structure. The actual breakdown associated with the current spikes is then sufficient to locally burn away the CNT. The elastomer in the vicinity of the burned-out CNT is then not connected to the percolating electrode network, reducing the available electrode area and hence the attainable capacitance and Maxwell stress. This is believed to be the origin of the slight reduction in the measured displacement in the first few cycles. It is noticeable that we cannot clear the soft breakdowns if the concentration of CNTs in the electrode is high, for

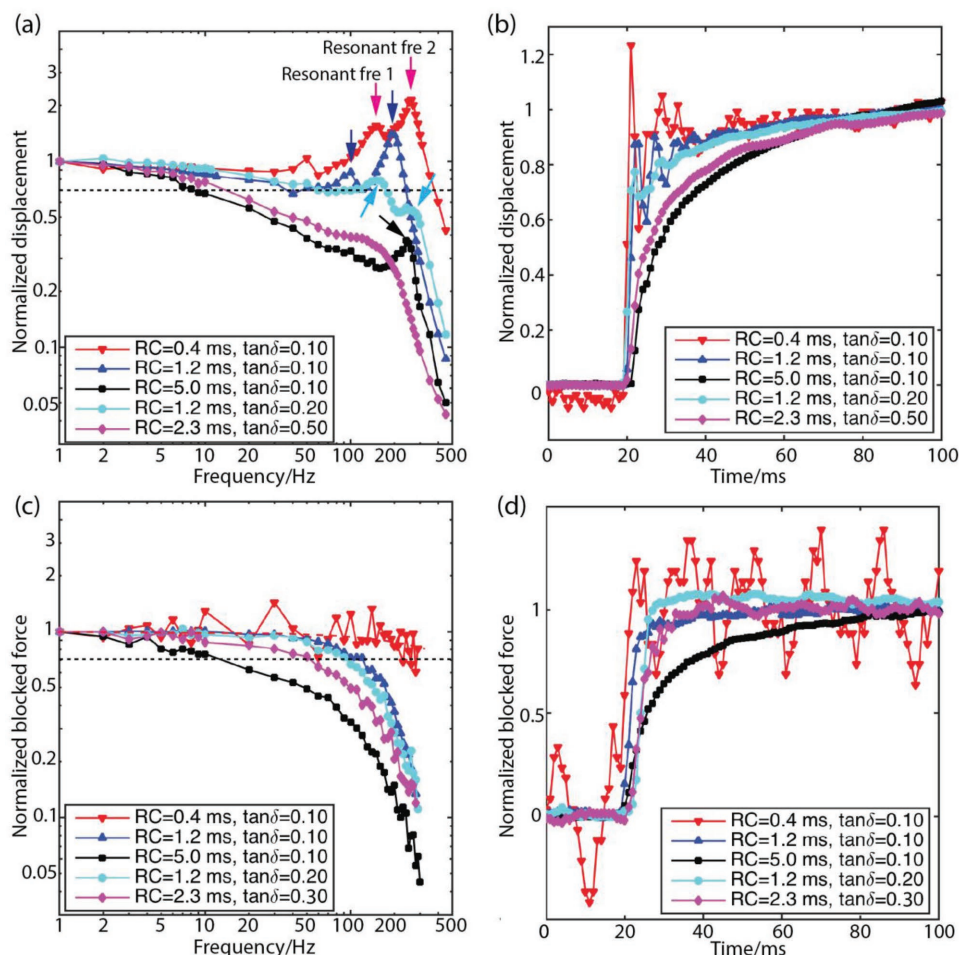


Figure 6. a) Displacement frequency response for the elastomer (varying $\tan \delta$)/electrode (varying RC) combinations indicated. b) Displacement response to a voltage step of 1 kV for the same combinations. c) Blocked force frequency response. d) Blocked force response to a voltage step of 1 kV for the same combinations. Note: the first combination was tested at 200 V.

instance “3 ×” in Table 1. We interpret this to mean that if the CNT concentration is too high, it is not possible to burn away the electrode in the vicinity of the breakdown so that path can continue to act as a short circuit when voltage is again applied. This, in turn, suggests that there is an optimum concentration: high enough to maintain a high conductivity and low RC constant but sufficiently low that soft breakdowns can clear away local imperfections.

Although we are able to create actuators with high bandwidth and power density, the quadratic dependence of the

attainable displacement with voltage suggests that much larger displacements (and forces) can be achieved at higher fields. However, for compatibility with our power supplies, we have arbitrarily limited the voltages to a maximum of 1000 V. This is well below the electrical breakdown voltages, which are limited by thickness of the elastomer layers and are also dependent on the CNT electrode concentrations.

In the majority of tactile applications, the actuator action is anticipated to be pushing into another material, such as skin. While the majority of conventional actuator designs are

Table 2. Dynamic response of different actuators.

Actuator	Elastomer	Electrodes	RC [ms]	$\tan \delta$ @ 1Hz	Resonant frequency 1	Resonant frequency 2	Free displacement bandwidth ^{a)}	Blocked force bandwidth ^{a)}
12	Mixture (1:1)	3× CNT	0.4	0.10	140 Hz	260 Hz	400 Hz	300 Hz
13	Mixture (1:1)	2× CNT	1.2	0.10	100 Hz	180 Hz	200 Hz	100 Hz
14	Mixture (1:1)	1× CNT	5.0	0.10	None	240 Hz	10 Hz	12 Hz
15	Sylgard 40:1	2× CNT	1.2	0.20	140 Hz	230 Hz	160 Hz	90 Hz
16	Sylgard 50:1	2× CNT	2.3	0.30	None	None	13 Hz	50 Hz

^{a)}Defined as the frequency at which the displacement amplitude drops to $\frac{\sqrt{2}}{2}$ of the static amplitude.

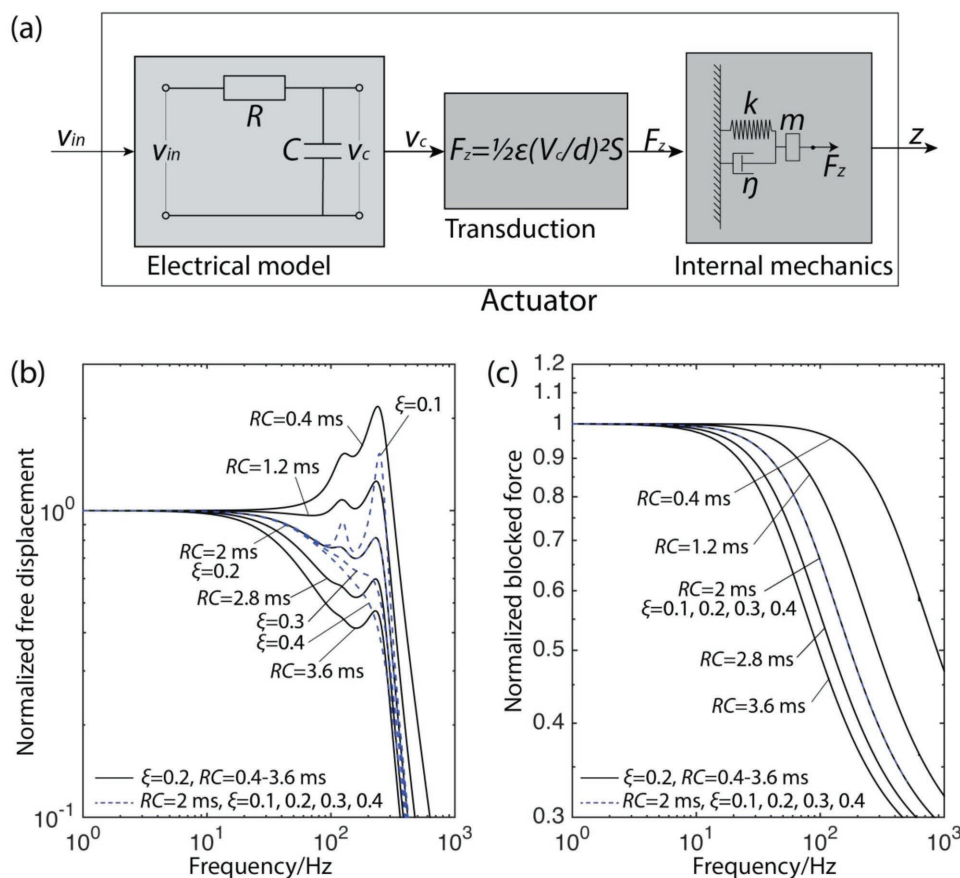


Figure 7. a) Block diagram of the actuator's dynamic model. b,c) Predicted frequency dependence of free displacements and blocked forces for a variety of electrical resistances and damping ratios, ξ . The parameters are derived from the measured elastomer and electrode parameters. Comparison should be made with the experimental data in Figure 6(a) for the normalized free displacements and with Figure 6(c) for the normalized blocking force.

agnostic to their application because they are constructed using very stiff materials, the low stiffness of soft robotic actuators raises other design considerations. Among these is the ability to resist buckling. Because the materials used are exceptionally soft (Table 3), dielectric elastomers actuators must also be designed to resist buckling even in haptic applications. This can be avoided by using short, low-aspect-ratio actuators, as in this work.

Another consequence of using a soft actuator is the importance of suppressing other competing deformation modes. One of these is a “breathing” mode in which the cross-section oscillates between two perpendicular elliptical shapes. This again can be suppressed by using thick walls, in our case using multiple turns of multilayers in the roll.

Another practical consideration in using dielectric elastomer actuators is that there will inevitably be a portion of their length that is “inactive.” For instance, to avoid electrical breakdown at the ends where the electrodes may overlap or where a portion of the length is fully constrained for attachment purposes. Insight into the effect of such an inactive length is provided by the simulations described earlier. Two limits can be identified. In one limit, the inactive length is fully constrained by glue or packaging. In the other, there is a length identical with the active portion of the actuator, for

instance absent electrodes, and so the displacements are those calculated from the active length alone. In the former case, the packaging simply reduces the effective length.

5. Conclusion

In this paper, a flexible manufacturing approach based on multilayering elastomer sheets and CNT electrodes, followed by rolling has been described. Combinations of different elastomer compositions, carbon nanotube electrodes, and geometries are investigated both analytically and experimentally, and optimized to meet performance characteristics appropriate to tactile display applications in both static mode and dynamic mode.

The electromechanical model presented in Section 2 makes a number of predictions that have been validated in this work. Specifically, in the absence of any load, the axial displacement varies as a square of the electric field and the blocked force varies linearly with the number of layers in the cross section. Consequently, the energy density, defined as the integral of the product of the attainable blocked force and the attainable free displacement, divided by the mass, should vary as the fourth power of the electric field. For the elastomers studied, which exhibit linear elastic behavior over the actuation strains

Table 3. Material properties.

Material ^{a)}	Modulus ^{b)} [kPa]	$\tan \delta @ 1\text{Hz}^c)$	$\tan \delta @ 10\text{Hz}^c)$	$\tan \delta @ 100\text{Hz}^c)$
Ecoflex 0030	105.9	0.085	0.140	0.169
E-S mixture 2:1 ^{d)}	99.5	0.086	0.179	0.270
E-S mixture 1:1 ^{d)}	77.6	0.105	0.235	0.343
E-S mixture 1:2 ^{d)}	70.1	0.112	0.264	0.414
Sylgard (40:1)	82.7	0.206	0.402	0.612
Sylgard (50:1)	25.4	0.298	0.605	0.903
VHB ^{e)}	299.9	0.659	0.997	1.176

^{a)}All samples were cylinders with 1 cm height and 1 cm diameter and were fully cured at temperature of 70 °C for 1 h; ^{b)}modulus was tested in compression using an Instron; ^{c)} $\tan \delta$ were tested in compression with a 100 mN precompression and dynamic mechanical data were collected under 1% strain, using a Bose 3200 DMA system; ^{d)}E: Ecoflex 0030, S: Sylgard 184 (40:1), the mixtures were prepared using a Thinky mixer; ^{e)}VHB samples were prepared by rolling VHB 4905 film into cylinder of 1 cm diameter and 1 cm height.

investigated, our highest energy density was 0.275 J kg⁻¹ with a corresponding power density of 55 W kg⁻¹ for our thinnest (25 micrometer) elastomer layers. As the field depends on the thickness of the elastomer, there is a strong motivation for decreasing the thickness and achieving higher fields and/or lower voltages. Furthermore, the dynamic response of the actuators we have fabricated is consistent with a simple spring and dash-pot model (Figure 7a) incorporating data from dynamic mechanical analysis (DMA) measurements on the elastic modulus and viscoelastic losses of the elastomer. (This is in contrast to previous models which have been based on fitting.^[17]) Together, the quasistatic and dynamic models provide guidance for the design of actuators for future applications in haptics, wearable robotics, soft robotics, and microrobotics, for instance, based on measured materials properties.

6. Experimental Section

Elastomers: Silicones were chosen as the dielectric elastomers. For comparison, pure Sylgard 184 having cross-linker ratios of 40:1 and 50:1 were also evaluated. Table 3 lists the material properties of the silicone compositions that were explored. Properties of VHB are also listed, a commercially available elastomer commonly used in dielectric elastomer devices. All compositions were mixed using Thinky Mixer (Model ARE310)^[18] for 60 s at 2000 rpm and then thermally cured in an oven at 70 °C for 1 h. Cylindrical samples were casted using 3D printed molds. During actuator fabrication process, thin films were prepared using spin coaters (Laurell Technologies Corporation) at a three-step spinning: 500 rpm for 15 s followed by 1000 rpm for 15 s followed by final speed (1000, 1500, and 2000 rpm for different thickness requirements) for 70 s.

Electrodes: High concentration inks (optical density 10 at 550 nm) of single-walled carbon nanotubes free of any polymeric or ionic surfactants were received from Nano-C Inc (Westwood, MA). The CNTs ink was filtered through a PTFE filter (Sartorius AG) to produce a mat of carbon nanotubes on the filter that could then be transferred by stamping onto the elastomer to form electrodes. The thickness of the CNT mats was selected so as to achieve a sheet resistance, measured by four-probe resistance measurements, of 10³–10⁴ Ω⁻¹. This range of CNT concentration was found to give an equivalent RC time constant of 1–2 ms so that the RC time constant would not limit the desired actuator bandwidth. Three CNT concentrations were chosen (1 ×, 2 ×, 3 × 100 μL ink volume) and they had sheet resistances of 2000, 5000, and 9000 Ω⁻¹, respectively.

Characterization: To evaluate the actuators as a function of voltage and frequency, the testbed shown schematically in Figure S3 in the Supporting Information was developed. The actuator under test was mounted on a flat substrate attached to an optical table (Figure S3a, Supporting Information) and the voltage-induced displacement was measured using a noncontact optical sensor (2100 Fotonic Sensor, MTI Instruments, Inc). The blocked force was measured in a similar configuration (Figure S3b, Supporting Information) but using a load cell (Nano 17, ATI Industrial Automation) attached to a rigid support. Observations of the actuator were also made using high-speed photography and infrared imaging. The high voltage supply (TREK 610E) was under computer control using a Labview program. The currents were measured directly using a DAQ board (National Instruments NI-USB-6002) connected to the current monitor of the TREK 610E supply.

Supporting Information

Supporting Information is available from the Wiley Online Library or from the author.

Acknowledgements

This work was supported by Facebook, Inc. through the Wyss Institute for Biologically Inspired Engineering at Harvard University.

Conflict of Interest

The authors declare no conflict of interest.

Keywords

bandwidth, multilayering, rolled dielectric elastomer actuators, static modeling, tactile displays

Received: June 24, 2018

Revised: August 6, 2018

Published online:

- [1] a) R. E. Pelrine, R. D. Kornbluh, J. P. Joseph, *Sens. Actuators, A* **1998**, *64*, 77; b) R. E. Pelrine, R. D. Kornbluh, Q. Pei, J. P. Joseph, *Science* **2000**, *287*, 836; c) R. Pelrine, R. Kornbluh, J. Joseph, R. Heydt, Q. Pei, S. Chiba, *Mater. Sci. Eng., C* **2000**, *11*, 89.
- [2] a) S. Shian, K. Bertoldi, D. R. Clarke, *Adv. Mater.* **2015**, *27*, 6814; b) D. Chen, Q. Pei, *Chem. Rev.* **2017**, *117*, 11239.
- [3] a) C. Keplinger, T. Li, R. Baumgartner, Z. Suo, S. Bauer, *Soft Matter* **2012**, *8*, 285; b) C. Keplinger, J.-Y. Sun, C. C. Foo, P. Rothmund, G. M. Whitesides, Z. Suo, *Science* **2013**, *341*, 984.
- [4] a) I. M. Koo, K. Jung, J. C. Koo, J.-D. Nam, Y. K. Lee, H. R. Choi, *IEEE Trans. Rob.* **2008**, *24*, 549; b) M. Matysek, P. Lotz, T. Winterstein, H. F. Schlaak, presented at *World Haptics 2009 – Third Joint EuroHaptics Conf. and Symp. on Haptic Interfaces for Virtual Environment and Teleoperator Systems*, Utah, USA, March **2009**; c) P. Lotz, M. Matysek, H. F. Schlaak, *IEEE/ASME Trans. Mechatronics* **2011**, *16*, 58.

- [5] F. Carpi, P. Chiarelli, A. Mazzoldi, D. De Rossi, *Sens. Actuators, A* **2003**, *107*, 85.
- [6] a) Z. Suo, *Acta Mech. Solida Sin.* **2010**, *23*, 549; b) A. Poulin, S. Rosset, H. R. Shea, *Appl. Phys. Lett.* **2015**, *107*, 244104; c) S. Rosset, H. R. Shea, *Appl. Phys. A* **2013**, *110*, 281; d) P. Dubois, S. Rosset, M. Niklaus, M. Dadras, H. R. Shea, *J. Microelectromech. Syst.* **2008**, *17*, 1072.
- [7] a) M. Duduta, R. J. Wood, D. R. Clarke, *Adv. Mater.* **2016**, *28*, 8058; b) X. Niu, H. Stoyanov, W. Hu, R. Leo, P. Brochu, Q. Pei, *J. Polym. Sci., Part B: Polym. Phys.* **2013**, *51*, 197.
- [8] M. Vatankhah-Varnoosfaderani, W. F. M. Daniel, A. P. Zhushma, Q. Li, B. J. Morgan, K. Matyjaszewski, D. P. Armstrong, R. J. Spontak, A. V. Dobrynin, S. S. Sheiko, *Adv. Mater.* **2017**, *29*, 1604209.
- [9] a) G. Kovacs, L. Düring, S. Michel, G. Terrasi, *Sens. Actuators, A* **2009**, *155*, 299; b) F. Carpi, C. Salaris, D. DeRossi, *Smart Mater. Struct.* **2007**, *16*, S300.
- [10] N. Kellaris, V. Gopaluni Venkata, G. M. Smith, S. K. Mitchell, C. Keplinger, *Sci. Robot.* **2018**, *3*, eaar3276.
- [11] a) Q. Pei, M. A. Rosenthal, R. E. Pelrine, S. Stanford, R. D. Kornbluh, in *Smart Structures and Materials 2003: Electroactive Polymer Actuators and Devices (EAPAD)*, Vol. 5051, Int. Society for Optics and Photonics, California, USA **2003**, p. 281; b) R. Zhang, P. Lochmatter, A. Kunz, G. M. Kovacs, presented at *SPIE Smart Structures and Materials + Nondestructive Evaluation and Health Monitoring*, Colorado, USA **2006**.
- [12] R. Sarban, R. W. Jones, B. R. Mace, E. Rustighi, *Mech. Syst. Signal Process.* **2011**, *25*, 2879.
- [13] J. Huang, T. Lu, J. Zhu, D. R. Clarke, Z. Suo, *Appl. Phys. Lett.* **2012**, *100*, 211901.
- [14] a) A. Israr, S. Choi, H. Z. Tan, presented at *2006 IEEE/RSJ Int. Conf. on Intelligent Robots and Systems*, Beijing, China, October **2006**; b) H. Olausson, J. Wessberg, I. Morrison, F. McGlone, *Affective Touch and The Neurophysiology of CT Afferents*, Springer, New York **2016**.
- [15] a) A. Rajamani, M. D. Grissom, C. D. Rahn, Q. Zhang, *IEEE/ASME Trans. Mechatronics* **2008**, *13*, 117; b) F. Carpi, D. De Rossi, *Mater. Sci. Eng., C* **2004**, *24*, 555.
- [16] a) H. Stoyanov, P. Brochu, X. Niu, C. Lai, S. Yun, Q. Pei, *RSC Adv.* **2013**, *3*, 2272; b) W. Yuan, L. Hu, Z. Yu, T. Lam, J. Biggs, S. M. Ha, D. Xi, B. Chen, M. K. Senesky, G. Gruner, Q. Pei, *Adv. Mater.* **2008**, *20*, 621.
- [17] R. Sarban, B. Lassen, M. Willatzen, *IEEE/ASME Trans. Mechatronics* **2012**, *17*, 960.
- [18] R. E. Pelrine, R. D. Kornbluh, J. Eckerle, P. Jeuck, S. Oh, Q. Pei, S. Stanford, presented at *Proc. SPIE Electroactive Polymer Actuators and Devices*, California, USA, **2001**.